TOWARDS OPERATIONAL MULTISENSOR REGISTRATION

ERIC J.M. RIGNOT, RONALD KWOK, and JOHN C. CURLANDER

Jet Propulsion Laboratory
California Institute of Technology
4800 Oak Grove Drive
Pasadena, CA 91109, U.S.A.
Ph (818)-354-1640
telex 675-429

Abstract. To use data from a number of different remote sensors in a synergistic manner, a multidimensional analysis of the data is necessary. However, prior to this analysis, processing to correct for the systematic geometric distorsion characteristic of each sensor is required. Furthermore, the registration process must be fully automated to handle a large volume of data and high data rates. In this paper, a conceptual approach towards an operational multisensor registration algorithm is presented. The performance requirements of the algorithm are first formulated given the spatially, temporally and spectrally varying factors that influence the image characteristics and the science requirements of various applications. Several registration techniques that fit within the structure of our algorithm are then presented. Their performance was evaluated using a multisensor test data set assembled from the Landsat TM, SEASAT, SIR-B, TIMS and SPOT sensors. The results are discussed and recommendations for future studies are given.

1. Introduction

In future years a number of spaceborne remote sensing instruments will be operational. These instruments will gather data over a broad range of the electromagnetic spectrum allowing scientists to study the physical, chemical and electrical properties of the Earth's environment on a global scale and over an extended period of time. To derive geophysical parameters of interest for each of the planned science applications, the data collected by these sensors must be combined and analyzed in a multidimensional manner. However, the sensors may be on different platforms and in different orbits, have different physical characteristics, viewing geometries, and data collection and processing systems. Consequently, systematic and nonsystematic registration errors will exist between coincident multisensor data samples. It is a prerequisite for synergistic analysis of these data to remove such errors. Furthermore, because of the anticipated large data volume and high data rates of future high resolution sensors, it is necessary to develop an automated multisensor registration process that requires no or little operator supervision.

Considerable experience has already been accumulated in the operational registration of Landsat data (e.g. Grebowsky, 1979). However, these techniques are not well adapted to the registration of image data from multiple sensors of significantly different characteristics operating at different wavelengths. A robust and adaptable automated multisensor registration technique must be developed.

In this paper, a high-level algorithm that integrates several registration techniques is presented. First, a formulation of the performance requirements for development of an operational algorithm is given. These requirements are derived from the needs of several key science applications as well as a review of practical limitations given the image characteristics. We then describe the multisensor test data set that has been assembled for evaluation of several computational techniques that fit within the structure of our algorithm. One registration technique that has been evaluated uses high resolution digital elevation models (DEM) of the areas to be registered. Others, which operate in the absence of ancillary data, are based on the extraction and matching of scene features across the different images to be coregistered. The results are discussed and recommendations for future work are given.

2. Performance Requirements

2.1 Characterization of the Input Data

A number of spatially, temporally and spectrally varying factors influence the image characteristics and the registration accuracy.

Due to the finite precision of the estimate of the platform ephemeris and attitude, absolute location errors and geometric distortion affect the geometric quality of the imagery. Such errors can typically be removed by the use of tiepoints. However, nonsystematic errors and tiepointing bias the image location, and a final step of precision registration is required to achieve sub-pixel level accuracy. The geometric quality of the data is also affected by the presence of topography in the observed scene. For an active sensor like a synthetic aperture radar (SAR), predominant terrain-induced geometric distortions such as foreshortening and layover (Lewis and Mc Donald, 1970) constitutes additional difficulties. Rectification of these distortions is essential before registration of the data. As an illustration, a perspective view of geocoded and rectified multisensor imagery is shown in Figure 1 using a technique described in (Kwok et al., 1987).

For sensors on different platforms and in different orbits, the acquired data are intially sampled to grids that are more natural to the sensor geometry than that of multisensor registration. A common grid for image coregistration, such as an Earth-fixed grid, is required. The process of mapping image data into this grid is

known as geocoding and has been developed for a variety of sensors including SAR (Curlander et al., 1987).

Multisensor registration will be affected by the large variability in spatial resolution of the data to be registered (from tens of meters (SAR, HIRIS) to kilometers (MODIS, HMMR) in the future NASA Earth Observing System (EOS) platform). Since resolution defines the ability of a system to discriminate small details within a scene, it establishes a limit for the achievable registration accuracy.

System noise (i.e. thermal noise, quantization noise, bit error noise, etc.) will also affect the registration accuracy, because many of the techniques used for registration are very sensitive to noise. While all sensors are corrupted by additive noise from the receiver electronics, SAR images are additionally corrupted by multiplicative noise known as image speckle. Thus the multisensor registration techniques must be robust to noise of a variety of statistics.

An additional consideration in any registration scheme is the scene composition. In cases where only a few features can be positively identified across the various sensors, the registration accuracy may be seriously inpaired. Furthermore, identifiable features are inherently space, time and frequency dependent. Therefore, it is necessary to develop robust automated techniques of selection of invariant features across the multisensor data.

In view of the above remarks, the input and output data requirements for an operational algorithm can be formulated. They define the operational domain and conditions under which the multisensor algorithm is expected to operate, and can be used as a basis for the evaluation of candidate algorithms.

2.2 Input and Output Data Requirements

The input data shall be corrected from the geometric distortion characteristic of each sensor using the best information available, geocoded onto a preselected grid common to all sensors (e.g. UTM), and resampled to the same pixel spacing. The signal to noise ratio of the data shall be better than 5 dB. The geodetic accuracy of the input images shall be better than 500 meters or 10-50 pixels. It is expected that most sensors will do better than this since most of them will have an accurate geographical location system on board.

The output products shall have a registration accuracy of less than one resolution element. This requirement is derived from a subset of application being considered for multisensor data analysis.

In the case of change detection, sub-pixel accuracy is desired to compare the response of individual pixel elements. Depending on the scene characteristics (presence of identifiable features) this requirement may be very difficult to achieve. In other cases, for example in the global study of hydrological cycles (which includes tasks such as sea-ice identification and dynamics, determination of moisture content of soil and vegetation, vegetation identification, areal extent and growth, etc.) a registration accuracy of several resolution elements may be sufficient.

It is important to point out that although the accuracy requirements have typically been well defined for each individual instrument, little or no accuracy requirements have yet been clearly defined for multisensor registration by the scientific community (EOS, 1987). More work is clearly needed in this area for each interdisciplinary science application.

3. Multisensor Test Data

A multisensor test data set has been assembled using image products from SEASAT SAR, SIR-B SAR, Landsat TM, SPOT, and TIMS (Kwok et al., 1989). Information on each sensor, including look angle, spectral range, polarization and spatial resolution is given in Table 1. Geocoding of the images to a common UTM Earth-grid has been performed and the data have been resampled to the same pixel spacing of 25 meters. Several sub-images of reduced size (512 x 512, 1024 x 1024 pixels) were selected from the areas where the sensors have coincident coverage. The characteristics of the original image data and of the selected sub-images are presented in Table 2. This table includes information about the geographic location of the data, the initial sample spacing and size, the revolution number and date of acquisition, the number of selected sub-images and the type of map projection used for coding. A summary list of the natural features present in the imaged scenes is also indicated.

For each selected sub-image, manual registration was performed, resulting in an estimated relative misregistration uncertainty of less than $\pm$ 2 pixels, roughly equal to the largest resolution element (40 meters). This uncertainty results from the differences in resolution between the various sensors. This estimate is used as a basis for the true registration for quantitative evaluation of the performance of various automated registration techniques.

4. Automated Multisensor Registration

The structure of the candidate multisensor registration algorithms is presented on Table 3. The input data satisfy the requirements as formulated in the previous section. The first processing step consists of automatically selecting sub-frames from each input image to define local areas of multisensor coincident coverage where pre-

cision registration can be performed with a high confidence of success. Depending on the availability of ancillary data (DEM or cartographic maps) a registration mode is selected. For the case where DEM is available the multisensor data are coregistered to the common grid provided by the DEM. Otherwise, invariant features are extracted from the sub-images and correspondence is established across the data to be registered. To reduce the computational complexity of the algorithm and obtain several estimates of the misregistration per sub-image, feature matching is performed at multiple locations and the results are then filtered to evaluate their relative spatial consistency within the selected patch (local constraints). If the match can be labeled as statistically significant (e.g. satisfies some goodness measure), the misregistration error of the selected sub-image is estimated and the multisensor data are then registered. Otherwise, the result is rejected and the selection and matching process is repeated with different parameters. At a higher-level of processing, the combined results from different features and from registered neighborhood patches (global constraints) can be used to produce a more accurate and more reliable solution. In effect, a cooperative process can be established where the results from different stages of the processing are used as reinforcements for the entire process.

Several candidate techniques which are effective within this structure are presented in the remainder of this section. They have been selected based on compatibility, robustness and adaptivity to the various sensors. Each matching algorithms' performance is assessed using the multisensor test data set described in the last section.

4.1 Automated Selection of Sub-images

Selection of the patches where fine registration is desired must be based on the extraction of stable features that can be unambiguously identified across the entire multisensor image data set. The difficulty is to formulate an approach without *a−priori* knowledge of the scene content. One possible technique has been described in (Davis and Kenue, 1978) where binary edge maps are used to compute a figure of merit for candidate control points. The results obtained with images from different sensors are then cross correlated to retain valid candidates.

4.2. Automated registration to digital terrain data

Our approach is to simulate multisensor imagery from a digital elevation model (DEM) of the area where the sensors have a coincident coverage and register this simulated imagery with the actual imagery, thereby inducing coregistration of the multisensor data on the common grid provided by the DEM.

Using elevation data, viewing geometry and a model of the scene reflectance, the appearance of the scene for any given sun angle and viewing angle can be simulated as in (e.g. Horn and Bachman, 1978) for passive sensors operating in the visible and near-visible part of the spectrum. An example of a synthetic image generated using this technique is shown in Figure 2. The illumination parameters were matched to a Landsat TM image data acquired over the same area. A simple matching technique (area-correlation) is then used to establish the correspondence between the images. The registration error is approximately 80 meters for the images shown.

Our approach to generate simulated SAR image from the DEM is similar to that described above. The sensor imaging geometry, the elevation data and a model of the radar backscatter are all required to produce the image shown in Figure 3. The imaging geometry simulates that of a SEASAT image acquired over the same area. An area correlation scheme is then used to match the radar and simulated images. Using tiepoint measurements of identifiable features not within the image shown, a misregistration error of 60 meters was obtained.

Several potential error sources affect the registration accuracy, including the the uncertainty in the actual imaging geometry, the geometric accuracy of the DEM data (height), and the reflectance model used for the optical data.

4.3 Computational Approaches

In the absence of reference maps, elevation data, geographical information or correlative ground truth information, blind techniques based on the identification of invariant features across the data can be used for image registration.

A. Feature extraction

Candidate features commonly used in digital imagery include edges, regions, lines, vertices of line intersection, shapes, etc. These features must be robust to change in sensor geometry, wavelength, SNR and noise statistics. Two particular types of features, region boundaries and edges, were examined using our multisensor data set.

Multisensor region boundaries extraction

Region boundaries are one of the simplest invariant low-level features than can be used to characterize the misregistration.

Even though many unsupervised segmentation techniques exist for optical images, most of them are not effective for SAR images because of the presence of speckle

noise. One unsupervised technique that seems to work reasonably well is a scheme based on a clustering algorithm to segment the images into several regions of similar intensity and texture (Kwok et al., 1989). The region boundaries are then established where a class transition occurs.

A resulting segmentation map, using 3 classes, is shown on Figure 4 together with the original images from SEASAT, Landsat, and SPOT. A 3 x 3 pixels window was used at each pixel location to compute the mean grey level and grey level texture via a simple standard deviation measure. The results obtained by matching these region boundaries are usually less accurate than those obtained with other techniques. However region segmentation can still be refined, especially in the case of SAR imagery, to provide information that complements results from other techniques.

Multisensor edge detection

An extensive literature exists on the subject of edge detection in optical imagery. However, in the case of SAR images the detection process is complicated since the images are corrupted by speckle noise. Techniques based on an approximation of the first and second directional derivatives (e.g. Sobel, or Robert operators) perform poorly, especially in terms of localization of the edges since they tend to produce large responses. Statistical edge operators (Touzi et al., 1988, Frost et al., 1982) in a lot of cases suffer from the same limitation.

This problem is solved by regularization techniques, specifically using a two-dimensional Gaussian smoothing operator as in a Marr-Hildreth operator (Marr and Hildreth 1980) or a Canny edge detector (Canny 1983). These operators typically have good detection and localization properties without multiple responses to a single edge, the three performance criteria for evaluation of edge detection algorithms. Theoretically, these techniques are compatible to almost all types of remote sensor data. Their performance with optical data have been documented in the literature (Marr and Hildreth 1980, Canny 1983).

The performance of these two operators was quantitatively compared in (Kwok and Rignot, 1989) in the case of synthetic SAR images as well as actual SAR images. It was shown that the gradient operator outperforms the Laplacian operator in both detection and localization of edges in image speckle.

Significant improvments in the performance of the ∇G operator can result from optimizing the parameter selections. In particular, the value of the filter spatial width σ must be adapted to the spatial resolution of the different sensors. Automatic thresholding is another important factor. In our implementation, a threshold with

hysteresis as in (Canny, 1983) is used to eliminate insignificant edges. Further post-processing such as thinning and contour-filling techniques have been shown to improve the quality of subsequent matches. Another possible improvement of the edge detector uses multiple operator widths and combines the resulting edges using a technique called feature synthesis, where the responses of the smaller operators are used to predict the response of a larger operator. Some results with optical images have been presented in (Canny 1983).

For illustration, one example of edge-map using SEASAT, Landsat TM and SPOT data and the Canny edge detector with a spatial width of 2 pixels (40 m) and adaptive thresholding is presented in Figure 5.

B. Feature Matching

Candidate feature matching techniques include binary cross correlation, distance transform / Chamfer matching, dynamic programming, and structural and symbolic matching.

In the case of region boundaries and edges a convenient binary representation of the feature maps can be used, a grey level of one at location of a feature-point and zero otherwise. This representation reduces the computational complexity of feature matching since computational cost becomes proportional to a linear dimension as opposed to area correlation where computational cost is proportional to an area.

Binary correlation

The binary feature-maps of each of the images to be registered can be cross correlated for various relative image shifts. The shift corresponding to the peak of the cross correlation will be an estimate of the actual misregistration between the images. The process is fast and can be efficiently implemented on an array processor or vectorizing computer.

Distance transform and Chamfer matching

The distance transform and Chamfer matching are described in (Barrow et al. 1977). In this method feature-points are matched by minimizing a generalized distance between them.

A distance transform is first applied to a binary feature-map, arbitrarilly refered as the source image. The result of this transformation is a distance map where the grey level of each pixel is a measure of the distance between the pixel and the nearest feature-point. For various values of the relative shift between the source and

the target images, the total distance between the feature points of the two images can be computed. This measure is the sum of the distance values read from the source image at each location of a feature-point in the target image. If matching were perfect, this distance would be zero. The relative shift that produces the smallest total distance corresponds to an estimate of the actual relative translational misregistration between the images to be registered.

This method is more robust to distortion or residual rotation effects than a binary correlation method.

Comparison of binary correlation and Chamfer matching

The time of computation of the binary correlation is less than the time of computation of Chamfer matching, typically in the ratio 1 to 4 for a search area of 100 x 100 pixels using a 512 x 512 pixel image. The tolerance to residual rotation effects is of 1 degree in the case of the binary cross correlation based on a maximum registration accuracy of 2 pixels. This tolerance is improved to 3 degrees when thicker edges are used (3 pixels wide instead of 1) (Wong, 1977). In the case of Chamfer matching the rotation tolerance is of 3 degrees. Better registration results (10 to 20 %) were consistently obtained by binary correlation as compared to Chamfer matching. The reason is that the quality metric used during Chamfer matching does not perform as well as expected with multisensor data due to the presence of non-matchable edges across the data, i.e. edges that appear in one image and not in the other. Their presence biases the total distance between feature points and significantly affects the accuracy, whereas the binary cross correlation is not affected by non-matchable edges.

Dynamic Programming

This iterative method, combined with an autoregressive model (AR), was used in the work by (Maitre and Wu, 1989) to register severely distorted optical images to a reference map without *a-priori* knowledge of the distortion. The two processes work at a different level. The AR model defines the deformation of the image at a pixel scale, and dynamic programming optimizes the search for best registration of an ordered sequence of features or primitives (usually edges) with a comparable sequence of features extracted from a reference map. The technique is robust in the presence of non-matchable edges. Good results are shown in (Maitre and Wu, 1989) using NOAA-7 satellite data.

This method has not been tested yet using the multisensor test data set, but offers good potential.

C. Constraint Filtering

In practice, matching is performed on small areas (typically 256 x 256 pixels or less) to minimize the distortion. Thus, the time of computation is also reduced and the number of estimates of the misregistration between the two images is increased. The resulting data must therefore be filtered to eliminate false matches. A clustering technique can be used where the cluster centroid corresponds to the estimated misregistration of the images.

At a higher level, results obtained from several feature matches are used to improve clustering of the data. Results from neighborhood patches can also be included.

4.4 Experimental Results

Twelve 512 x 512 pixel images corresponding to 3 different geographic areas have been registered. Each image was divided into 4 sub-blocks, and the search area for the local registration shift was 101 x 101 pixels in each sub-block.

In the case of the images from SEASAT and SPOT, the rate of success of the binary correlation of edges was 87 %, and increased to 92 % after constraint filtering, with no false matching. In the case of images from SEASAT and Landsat TM, the rate of success of the same technique was 85 % before constraint filtering, and 86 % after. Registration was qualitatively more difficult in that case because of the lower resolution of the Landsat images as compared to SPOT images, and also because a few additional scenes where registration was more difficult was used.

The registration accuracy of the multisensor data was approximately $\pm$ 2 pixels (40 m). The achievability of sub-pixel accuracy seemed difficult to establish by visual inspection of our multisensor test data set, a fact that is a common problem when comparing digital imagery from multiple remote sensors.

5. Conclusions and recommendations

It is of considerable importance to develop automated multisensor registration tools for synergistic use of the data from a variety of spaceborne sensors. A high level algorithm that integrates a variety of registration techniques in a systematic manner was presented in this paper. It was tested using a somewhat limited multisensor test data set. A more complete study would enlarge this data set to include more instruments and more scene types. Additional techniques for feature extraction and feature matching also need to be evaluated in a follow-on study.

The performance of a multisensor registration algorithm is dependent on the sci-

ence requirements of the particular applications as well as the characteristics of the instrument, the imaged surface and the environmental conditions. This very complex task cannot be solved with just a single technique, but will require combining several techniques together that work in a competitive-cooperative mode of interaction. For this reason it seems logical that a rule based artificial intelligence approach may be necessary for the high level algorithm to select the optimal techniques and parameters from a particular multisensor application.

Acknowledgment

The authors wish to thank R. Fätland for his contributions to the software development effort and A. Pang and J. Weirick for their data processing support. This work was carried out under contract with the National Aeronautics and Space Administration at the Jet Propulsion Laboratory, California Institute of Technology.

References

Barrow, H. G., J. M. Tenenbaum, R. Bolles, H. C. Wolf, 1977, Parametric Correspondence and Chamfer Matching: Two New Techniques for Image Matching. *Proc. 5th Joint Conf. on Artificial Intelligence, Cambridge, Mass., 1977*, 659-663.

Canny, J. F., 1983, Finding edges and lines in images. Artif. Intell. Lab., Mass. Inst. Technol., Cambridge, MA. Tech Rep. AI-TR-720.

Curlander J. C., R. Kwok and S. Pang, 1987, A Post-Processing System for Automated Rectification and Registration of spaceborne SAR Imagery, *Int. Journal of Remote Sensing*, **8**, 4, 621-638.

Davis, W. A. and S. K. Kenue, 1978, Automatic Selection of Control Points for the Registration of Digital Images, *Proc. of the Int. Joint Conference on Pattern Recognition, 4^{th}, Kyoto, Japan, Nov 7-10 1978*, 936-938.

EOS Earth Observing System Reports, NASA Techn. Memorandum 86129, Vol. I and Vol II, NASA Publish., 1987.

Frost V. S., K. S. Shanmugan, and J. C. Holtzman, 1982, Edge Detection for Synthetic Aperture Radar and other Noisy Images. *Digest from the Intl. Geoscience and Remote Sensing Symposium.*

Grebowsky, G. J., 1979, Lacie Registration Processing, *The LACIE Symposium, Proceedings of the Technical Sessions, July 1979*, 87-97.

Horn B.K.P. and B. L. Bachman, 1978, Using synthetic images to register real images with surface models, *Comm. ACM, 11 Nov. 1978*, **21**, 914-924.

Kwok, R., J. C. Curlander and S. Pang, 1987, Rectification of Terrain Induced Distortion in Radar Imagery, *Photogrammetric Engineering and Remote Sensing*, **53**, 5, 507-513.

Kwok, R. and E. Rignot, 1989, Comparison of the $\nabla^2 G$ and ∇G Operators for Edge Detection in Speckle Noise, unpublished.

Kwok, R., E. Rignot, J.C. Curlander and S. Pang, 1989, Multisensor Image Registration: A Progress Report, Jet Propulsion Laboratory Internal Report JPL D-6697, September 1989.

Lewis, A.J. and H.C. Mac Donald, 1970, Interpretive and mosaicking problems of SLAR imagery, *Remote Sens. Environ.*, **1**, 213.

Maitre, H. and Wu, Y., 1989, Dynamic programming algorithm for elastic registration of distorted pictures based on autoregressive model, *IEEE Trans. on Acoust., Speech, and Sign. Proc.*, **37**, 2, 288-297.

Marr, D. and E. Hildreth, 1980, Theory of edge detection. *Proc. Royal Soc. London*, B, **207**, 187-217.

Touzi, R., A. Lopes and P. Bousquet, 1988, A Statistical and Geometrical Edge Detector of SAR Images. *IEEE Trans. Geosci. and Remote Sens.*, **26**, 6, 826-831.

Wong, Y. R., 1978, Sequential Scene Matching using Edge Features. *IEEE Trans. on Aerospace and Elect. Systems*, **14**, 1, 128-140.

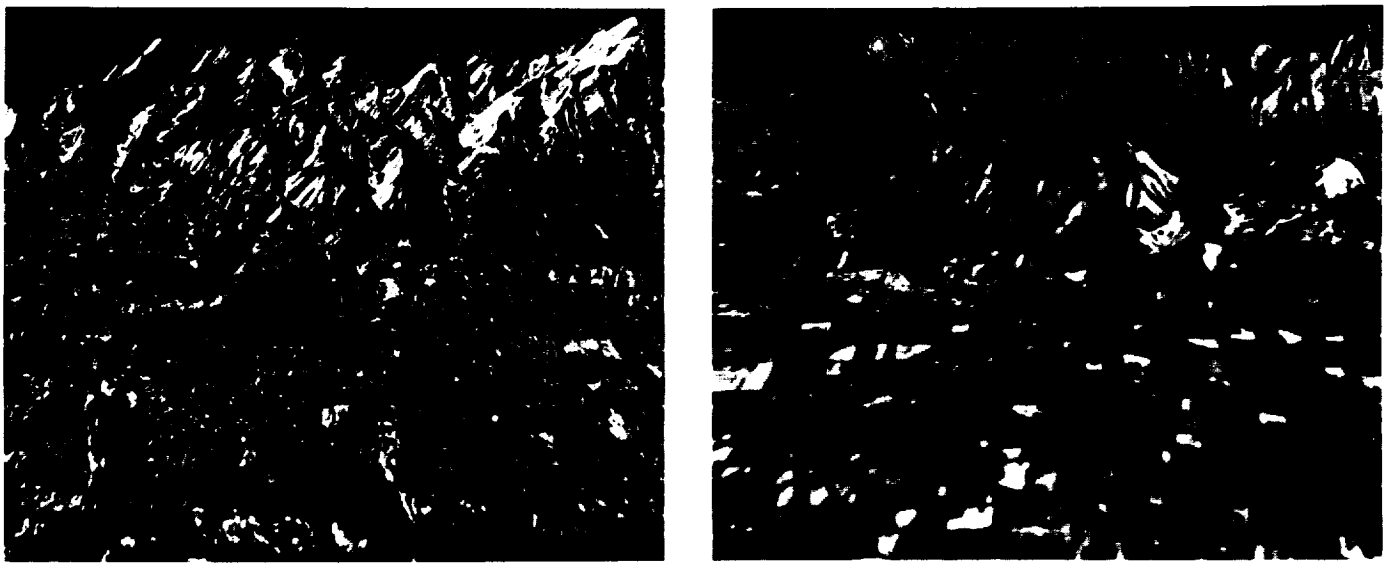

(a) (b)

Fig. 1. Perspective viewing of multisensor geocoded and rectified images of an area near Los Angeles, California: (a) SEASAT radar image; (b) Landsat TM, band 4, image.

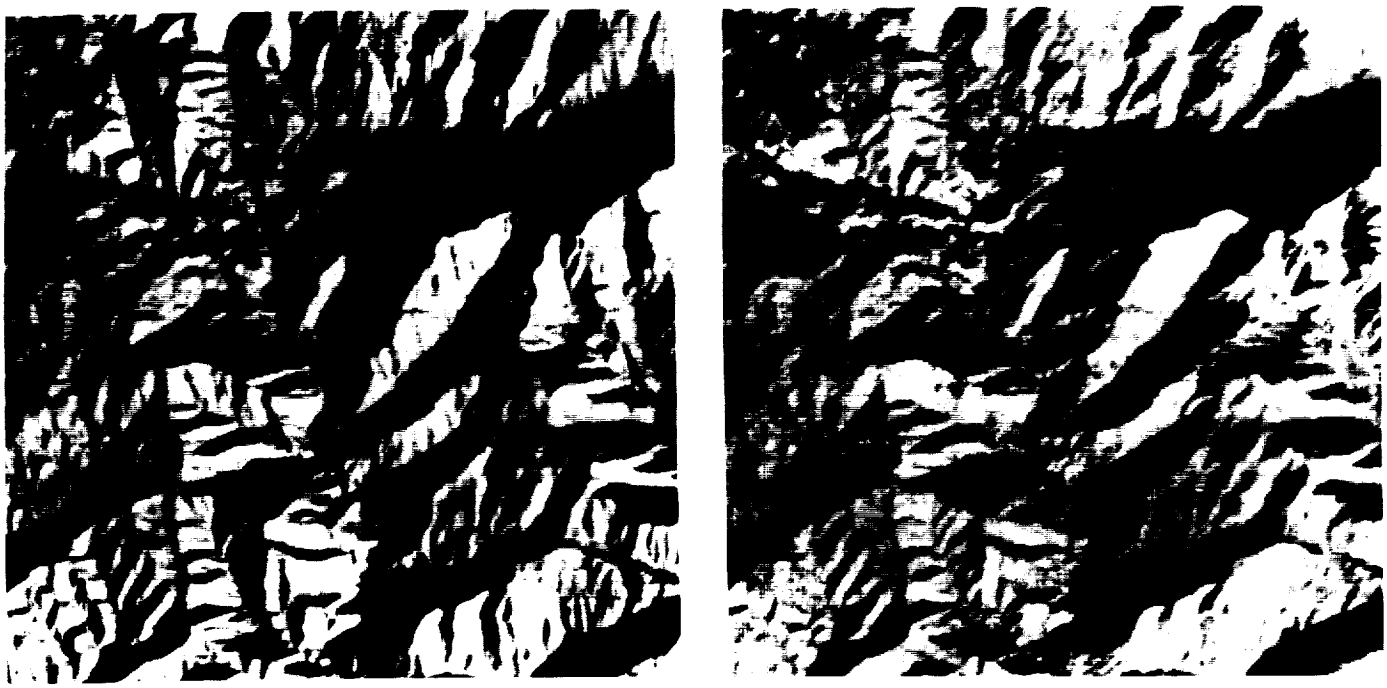

Fig. 2. Comparison of simulated versus actual Landsat TM image: (a) simulated image: (b) actual image.

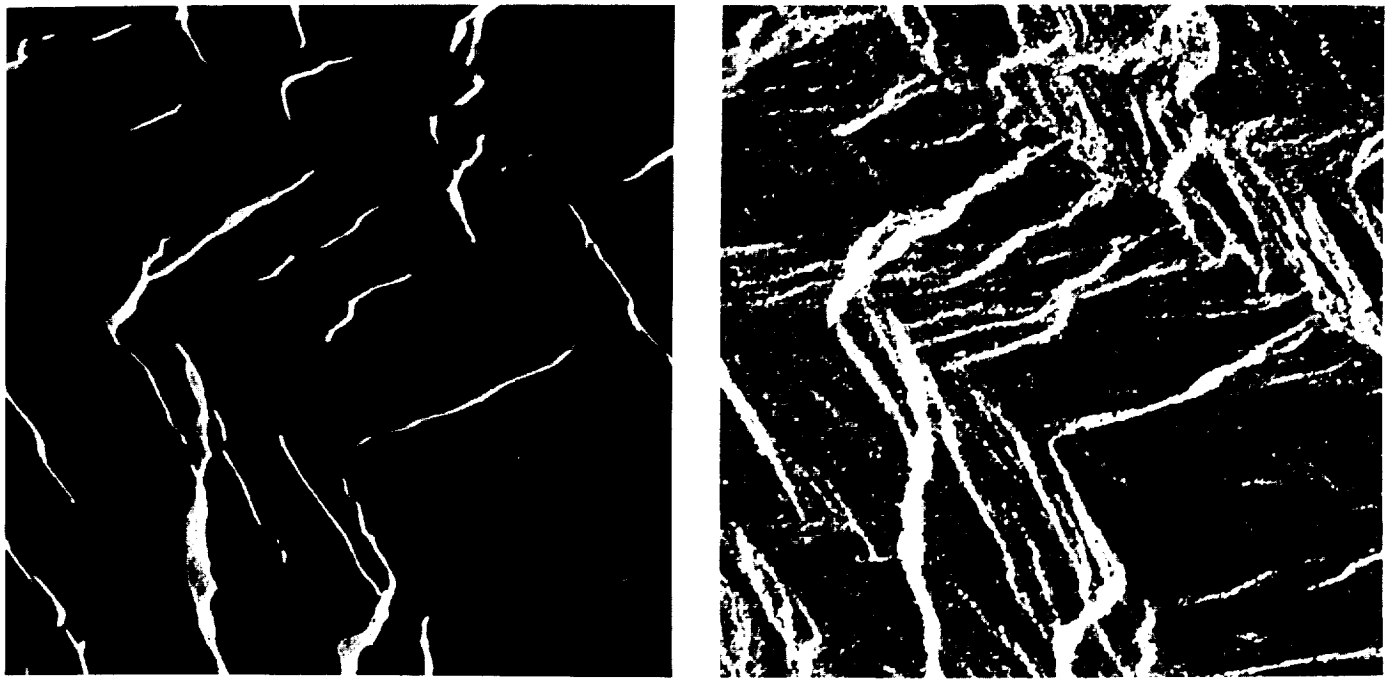

Fig. 3. Comparison of simulated versus actual SEASAT radar image: (a) simulated image: (b) actual image.

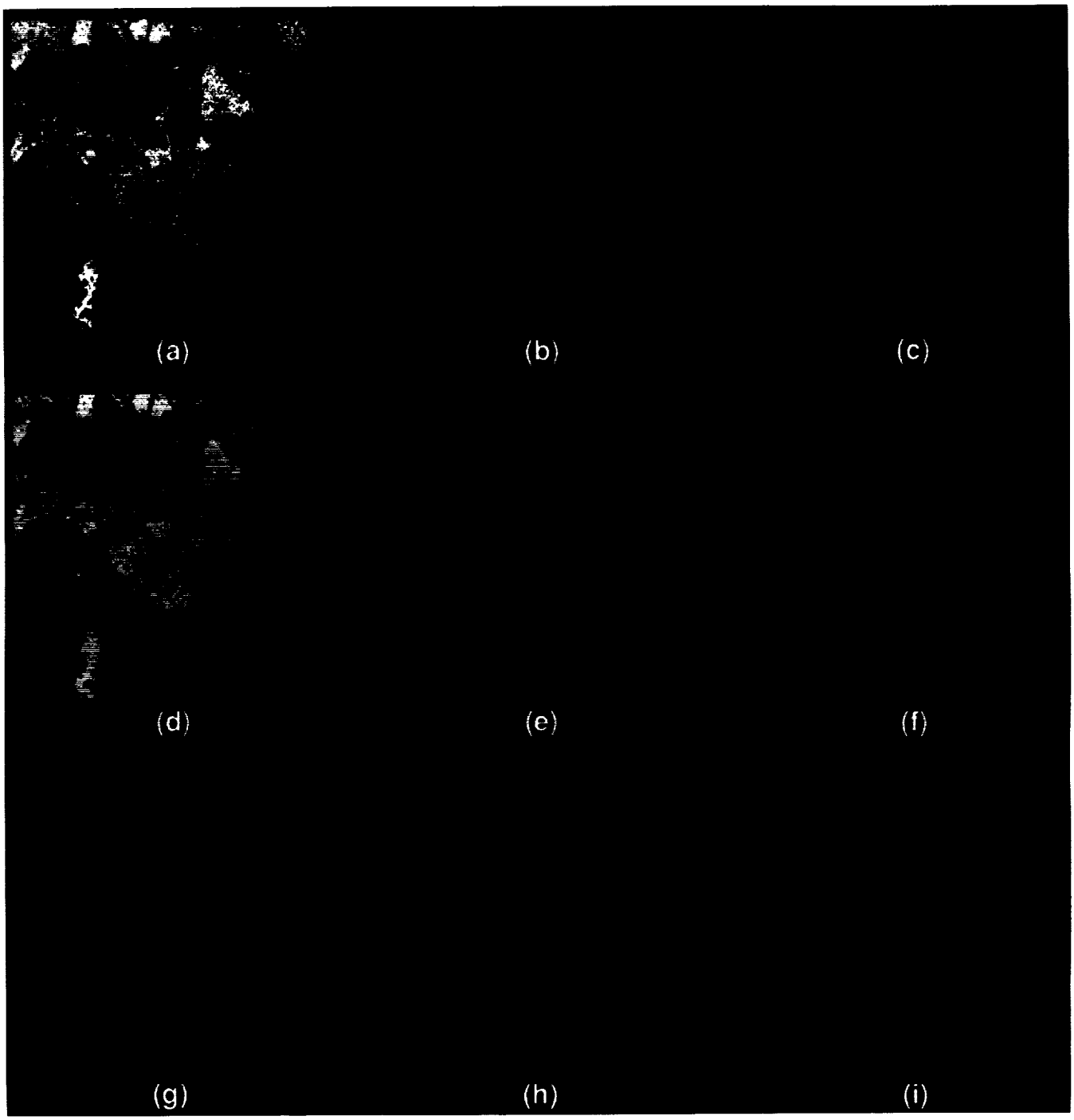

Fig. 4. Unsupervised segmentation of Optical and SAR images from an area near the Altamaha River, Georgia. (a) SEASAT, (b) Landsat TM, and (c) SPOT images are segmented into 3 regions represented in (d), (e), and (f) respectively. The corresponding images of region boundaries are (g), (h), and (i) respectively.

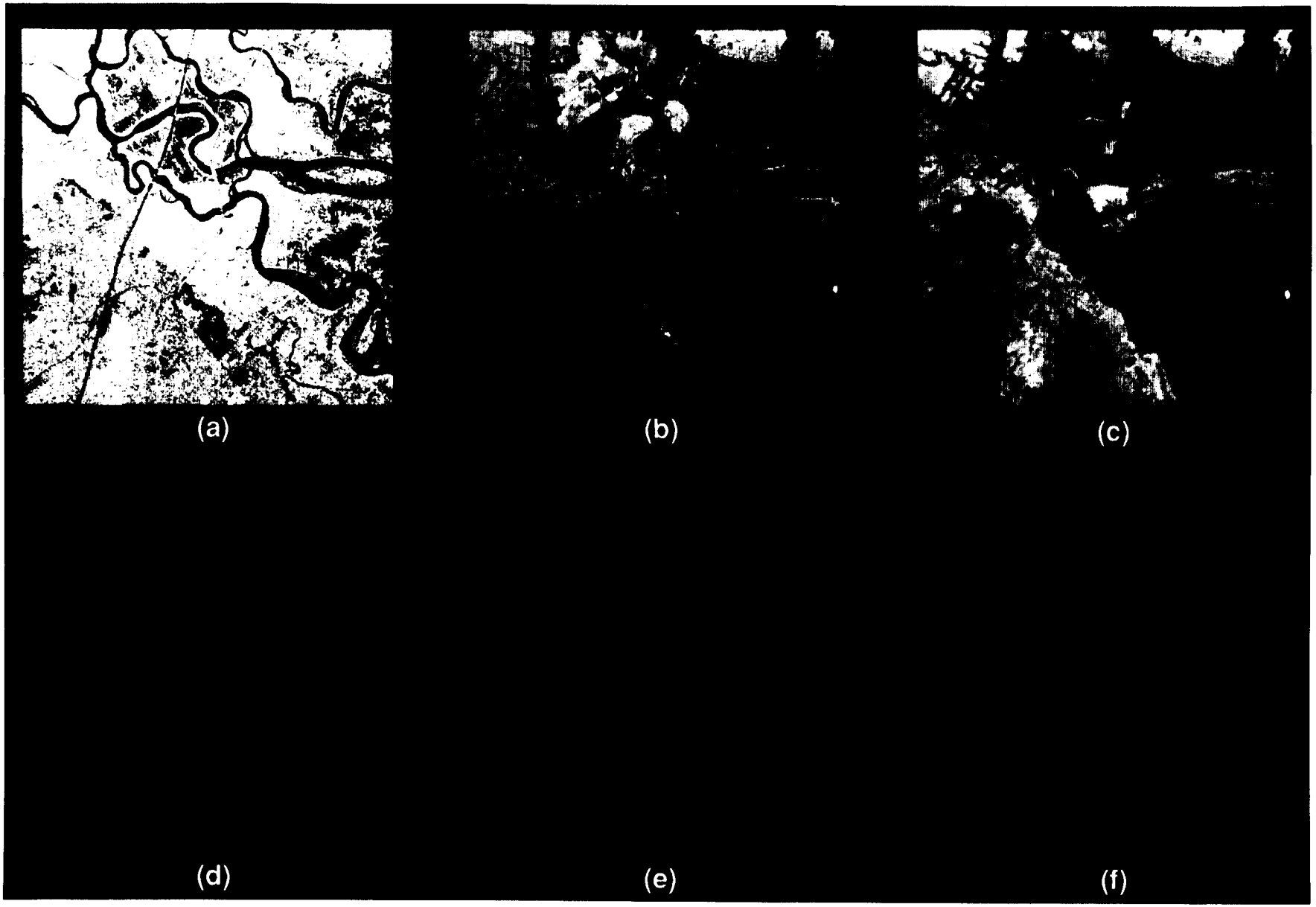

Fig. 5. Edge detection in (a) SEASAT, (b) Landsat TM, and (c) SPOT images of an area near the Altamaha River, Georgia. The edge-maps obtained from Canny's edge detector are represented in (d), (e), and (f) respectively.

Table 1. Description of the characteristics of the different sensors involved in the constitution of the multisensor test data set.

JPL MULTISENSOR TEST DATASET

NAME OF SENSOR	TYPE	FREQUENCY	RESOLUTION (ORIGINAL DATA)
SEASAT	SAR ACTIVE	L BAND, HH POLARIZATION 23 ° LOOK-ANGLE	25 m
SIR-B	SAR ACTIVE	L BAND, HH POLARIZATION 15 TO 60 ° LOOK-ANGLE	25 m
TIMS	RADIOMETER PASSIVE	THERMAL-INFRARED	30 m
LANDSAT TM	OPTICAL PASSIVE	7 BANDS SPECTRAL RANGE: 1 .45 µm - .52 µm; 2 .52 µm - .60 µm; 3 .63 µm - .69 µm; 4 .76 µm - .90 µm; 5 1.55 µm - 1.75 µm; 6 1.04 µm - 1.25 µm; 7 2.08 µm - 2.35 µm	28.5 m (pixel spacing) IFOV
SPOT	OPTICAL PASSIVE	3 BANDS SPECTRAL RANGE: 1 .50 µm - .59 µm; 2 .61 µm - .68 µm; 3 .79 µm - .89 µm	20 m (pixel spacing) IFOV

Table 2. Description of the multisensor test data set.

JPL

MULTISENSOR TEST DATASET

IMAGE FRAMES LOCATION	SEASAT	LANDSAT	SPOT	TIMS	FEATURES IN PATCHES
ALTAMAHA RIVER, GEORGIA (pixel size = 20 m)	Rev : 407 Date: Jul 78 Size: 5 K x 5 K Map Proj. : UTM # of patches selected for testing: 12	Date: Jul 84 Size: 3 K x 4 K Rotated to North # of patches selected for testing: 12	Date: Sept 84 Size: 3 K x 5 K Rotated to North # of patches selected for testing: 12		Rivers, Lakes, Fields, Roads, Coasts.
WIND RIVER BASIN, WYOMING (pixel size = 30 m)	Rev : 781 Date: Aug 78 Size: 5 K x 5 K Map Proj. : UTM # of patches selected for testing: 5	Date: Jun 84 Size: 5 K x 5 K Rotated to North # of patches selected for testing: 13			Mountains, Rivers, Lakes, Fields, Roads, Cities,
YUMA, ARIZONA (pixel size = 25 m)	Rev : 681 Date: Aug 78 Size: 3 K x 3 K Map Proj. : UTM # of patches selected for testing: 13	Date: Jun 84 Size: 3 K x 4 K Rotated to North # of patches selected for testing: 13			Mountains, Rivers, Fields, Roads, Cities, Dunes.
DEATH VALLEY, CALIFORNIA (pixel size = 25 m)	Rev : 882 Date: Aug 78 Size: 5 K x 5 K Map Proj. : UTM # of patches selected for testing: 4	Date: Nov 82 Size: 3 K x 4 K Rotated to North # of patches selected for testing: 4		Date: Jul 83 Size: 1 K x 1 K Rotated to North # of patches selected for testing: 4	Mountains, Fields.

Table 3. Flow chart of the multisensor registration algorithm.